DOI: 10.1021/ma101728w

Macromolecules
ARTICLE

# Steric Interaction between Flexible Main Chain and Nonmesogenic Cyclic Pendants Leading to Thermotropic Liquid Crystalline Property

**Xue Mei, Yang Chu, Jiaxi Cui, Zhihao Shen,* and Xinhua Wan***

*Beijing National Laboratory for Molecular Sciences, Key Laboratory of Polymer Chemistry and Physics of MOE, College of Chemistry and Molecular Engineering, Peking University, Beijing 100871, China*

*Received July 29, 2010; Revised Manuscript Received September 26, 2010*

ABSTRACT: Nonmesogenic cyclic alkylidene terephthalate is directly connected to flexible polyethylene main chain at every second carbon atom via the phenyl ring to obtain a novel vinyl polymer, poly(alkylidene vinylterephthalate) (PAVT-*n*), where *n* (= 10−14 and 16) denotes the number of methylene groups in the side chain. When the molecular weight is large enough, stable hexagonal columnar phases are generated from melt by the PAVT-*n* polymers with *n* = 10−13, but not by those containing 14 or 16 methylene groups. Compared with its open-ring counterpart, i.e., poly(dialkyl vinylterephthalate) (PDAVT-*n*) with linear side chains, PAVT-*n* has a glass transition temperature ($T_g$) over 100 °C higher, a much larger persistence length, and a much lower critical molecular weight to form a mesophase. In addition, PDAVT-*n* enters into isotropic liquid at $T_g$ and becomes ordered at temperatures well above $T_g$, whereas PAVT-*n* forms mesophases immediately above $T_g$. The strong steric interaction between cyclic pendants and the flexible main chain, which causes PAVT-*n* to take an extended chain conformation, is considered as the main driving force for PAVT-*n* to generate mesophases. In a sharp contrast, the mesophase formation of PDAVT-*n* is known to be an entropy-driven process.

## Introduction

Liquid crystalline polymers (LCPs) are fascinating organic materials that have found wide applications in high-strength and high-modulus fibers,[1] engineering plastics,[2] optical displays,[3] electro-optical modulators,[4] smart windows,[5] and so forth. LCPs are usually made up of rodlike or disklike mesogens either incorporated into the polymer main chains or appended as side chains through flexible spacers. The necessity of mesogens in the construction of LCPs makes them quite expensive and severely limits their macromolecular design and applications. One growing interest in this field is to design LCPs without bearing any conventional mesogens. By taking advantages of the self-assembly of cone-shaped side groups, Percec and co-workers achieved ordered dendronized polymers with the tubular helical chain conformation, where the arrangement possessed an ordered cylindrical structure.[6−8] Other examples include thermotropic poly(di-*n*-alkylsiloxane)s[9] by Möller and poly[dialkyl vinylterephthalate]s (PDAVT-*n*) with linear side chains[10] along with other polystyrene-based polymers by us.[11−13] The mesophase formation in these polymers is entropy-driven; i.e., the increased entropy caused by increased movements of disordered side chains overcompensates the reduction in entropy caused by the ordered arrangement of the main chain when the polymer enters into the liquid crystalline (LC) phase during the heating process. Within this scenario, the free terminals of alkyl chains play an important role in generating ordering of the polymer chain as a whole. Therefore, it is reasonable to ask what will happen if the two terminals of alkyl tails in the same repeating unit are covalently linked and how the resultant polymers behave.

To answer this question, in this article, a series of novel vinyl polymers, poly[alkylidene vinylterephthalate] (PAVT-*n*), where *n* (= 10−14 and 16) denotes the number of methylene groups in the side chain, are synthesized and characterized. Although the cyclic pendants are nonmesogenic and contain no free alkyl chains, the polymers display stable hexagonal columnar ($\Phi_H$) phases depending on their molecular weights (MWs) and sizes of side groups. Compared with its open-ring counterparts, PDAVT-*n* with linear side chains, PAVT-*n* shows remarkably different properties. The glass transition temperature ($T_g$) of the latter is over 100 °C higher than that of the former when the number of carbon atoms in the aliphatic side group is the same. In addition, the critical MW for PAVT-*n* to generate a mesophase is much lower than that for PDAVT-*n*. Moreover, PAVT-*n* enters into the mesophase immediately above glass transition, while PDAVT-*n* becomes isotropic melt first and then forms an ordered structure at the temperature much higher than $T_g$. This evidence suggests that the two kinds of polymers have distinct mechanisms in generating mesophases, although they show almost identical mesomorphic structures.

Low-MW cyclic polyethers like crown ethers have been employed to build either liquid crystals or LCPs.[14,15] The intention is to introduce additional assembling property into thermotropic liquid crystals or help generate mesophases by adjusting the conformation of building blocks through molecular recognition. Except for poly(dicycloalkyl vinylterephthalate) reported by us,[16,17] so far no other thermotropic LCPs containing flexible cyclic pendants are known.

## Experimental Section

**Materials.** 1,8-Octanediol, 1,9-nonanediol, 1,10-decanediol, 1,11-undecanediol, 1,12-dodecanediol, 1,13-tridecanediol, 1,14-tetradecanediol, and 1,16-hexadecanediol were all purchased from Isomersyn Technology Co. and used as received. Their purities were higher than 94%. Ethyl 2-bromo-2-methylpropionate (EBMP, Acros, 99%) and *N*,*N*,*N*′,*N*′,*N*″-pentamethyldiethylenetriamine (PMDETA, Aldrich, 99%) were used as received. Vinylterephthalic acid was synthesized according to the procedure reported previously.[18] Chlorobenzene (BzCl) was purified by washing with concentrated sulfuric acid to remove thiophene, followed by washing with water, and then dried over 24 h and distilled. Cuprous bromide (CuBr) was synthesized

*To whom correspondence should be addressed: Tel 86-10-6275 4187, Fax 86-10-6275 1708, e-mail xhwan@pku.edu.cn (X.W.); Tel 86-10-6275 4518, Fax 86-10-6275 1708, e-mail zshen@pku.edu.cn (Z.S.).

 Published on Web 10/13/2010 

from $CuBr_2$ and purified by stirring in glacial acetic acid, washing with methanol, and drying under vacuum. Benzoyl peroxide (BPO) was purified by precipitation from a chloroform solution into methanol and dried in vacuum at room temperature for 12 h before use. Tetrahydrofuran (THF) and $Et_3N$ were refluxed over $CaH_2$ and distilled out before use. 1,4-Diazabicyclo-[2,2,2]octane (DABCO) was sublimed just before use. Dimethylacetamide (DMAc) was dried by magnesium sulfate and distilled before use. $CH_2Cl_2$ was dried over anhydrous $CaCl_2$ for 24 h and distilled out. Other solvents and reagents were purchased from Beijing Chemical Co. and used without any purification unless otherwise specified.

**Instruments and Measurements.** $^1H$ NMR spectra of the monomers were obtained with a Bruker ARX300 spectrometer. $^1H$ NMR and $^{13}C$ NMR spectra of PAVT-12 were obtained with a Bruker ARX400 spectrometer at 400 and 100 MHz, respectively. $CDCl_3$ was used as the solvent and TMS as the internal standard. Heteronuclear multiple quantum coherence (HMQC) spectroscopy and nuclear Overhauser effect spectroscopy (NOESY) were obtained with a Bruker ARX400 spectrometer by using $CDCl_3$ as the solvent. Elemental analyses were carried out by means of a Carlo Erba 1106 instrument. Mass spectra were taken by a VG-ZAB-HS mass spectrometer.

The number-average molecular weight ($M_{n,GPC}$), weight-average molecular weight ($M_{w,GPC}$), and polydispersity index ($PDI_{GPC} = M_{w,GPC}/M_{n,GPC}$) of the resultant polymers were estimated on a gel permeation chromatographic (GPC) instrument equipped with a Waters 515 HPLC pump and a Waters 2410 refractive-index detector. Three Waters Styragel columns with 10 $\mu$m bead size were connected in tandem. Their effective molecular weight ranges were 100−10 000 for Styragel HT2, 500−30 000 for Styragel HT3, and 5000−600 000 for Styragel HT4. The pore sizes were 50, 100, and 1000 nm for Styragels HT2, HT3, and HT4, respectively. THF was used as the eluent at a flow rate of 1.0 mL/min at 35 °C. The calibration curve was obtained with polystyrene standards.

The absolute number-average molecular weight ($M_{n,GPC\text{-}LS}$), weight-average molecular weight ($M_{w,GPC\text{-}LS}$), and polydispersity index ($PDI_{GPC\text{-}LS} = M_{w,GPC\text{-}LS}/M_{n,GPC\text{-}LS}$) of the resultant polymers were also characterized by the same GPC instrument mentioned above using a Wyatt Technology DAWN HELEOS 18-angle (from 15° to 165°) light scattering detector with a Ga−As laser (658 nm, 40 mW). The concentration at each elution volume was determined with a Wyatt Optilab Rex interferometeric differential refractometer (658 nm). The molecular weight data were calculated using Astra 5.1.6.0 software (Wyatt Technology). The refractive index increment ($dn/dc$) of PAVT-12 was estimated as 0.169 mL/g in THF at 35 °C. The sample concentrations were 1.0, 2.0, 3.0, 4.0, and 5.0 mg/mL. The refractometer was calibrated with aqueous NaCl solutions. All samples were dissolved in THF and left overnight before filtration through a 0.45 $\mu$m PTFE filter.

The thermal transitions of the polymers were detected using differential scanning calorimetry (DSC) on a TA Q100 calorimeter in a temperature range of 0−280 °C at a heating rate of 20 °C/min under a continuous nitrogen flow. Glass transitions were determined by the second heating process after cooling at 2 °C/min from 220 °C. *n*-Octane (mp 56.8 °C) and indium (mp 156.8 °C) were used to calibrate the instrument. The average sample mass was about 6 mg, and the nitrogen flow rate was 50 mL/min. Thermogravimetric analysis (TGA) was performed on a TA Q600 instrument at a heating rate of 10 °C/min under a nitrogen atmosphere.

Polarized light microscopy (PLM) was conducted on a Leica DML polarized light optical microscope coupled with a Linkam TH-600PM hot stage. The sample films were prepared by solution-casting, and the thickness was kept at several micrometers.

One-dimensional wide-angle X-ray diffraction (1D WAXD) powder experiments were performed on a Philips X'Pert Pro diffractometer with a 3 kW ceramic tube as the X-ray source (Cu K$\alpha$ radiation) and an X'celerator detector. To study the structure evolutions as a function of temperature, a temperature control unit connected with the diffractometer was employed. Background scattering was recorded and subtracted from the sample patterns.

**Synthesis of Monomers. 1,12-Dodecylidene Vinylterephthalate (AVT-12).** A 100 mL flask was introduced with vinylterephthalic acid (2.0 g, 10.4 mmol), oxalyl chloride (30 mL), and several drops of DMF. The mixture was stirred at room temperature for 24 h. After evaporation of excess oxalyl chloride, $CH_2Cl_2$ was added. Vinylterephthaloyl chloride was used directly after complete evaporation of the solvents. A 500 mL two-necked Morton flask equipped with a magnetic stirrer and two pressure-equalizing dropping funnels was charged with DABCO (0.050 g, 0.44 mmol) and $CH_2Cl_2$ (50 mL). Solutions of vinylterephthaloyl chloride (2.06 g, 9.0 mmol) in 200 mL of $CH_2Cl_2$, 1,12-dodecanediol (1.82 g, 9.0 mmol), and a solution of $Et_3N$ (4.4 mL, 32 mmol) in 200 mL of THF were added dropwise via the two dropping funnels, at the same rate, in about 4 h. After the addition of the reagents, the reaction mixture was stirred for 4 h at room temperature and then filtered. Following evaporation of the solvents, the residue was separated from linear products by column chromatography eluted with $CH_2Cl_2$. AVT-12 was a light yellow solid. Yield: 30%. Melting point: 30 °C.

1,10-Decylidene vinylterephthalate (AVT-10), 1,11-undecylidene vinylterephthalate (AVT-11), 1,13-tridecylidene vinylterephthalate (AVT-13), 1,14-tetradecylidene vinylterephthalate (AVT-14), and 1,16-hexadecylidene vinylterephthalate (AVT-16) were prepared with the similar procedure to that for preparing AVT-12. Because of the poor solubility of 1,14-tetradecanediol and 1,16-hexadecanediol in $CH_2Cl_2$, DMAc was used as the solvent for the synthesis of AVT-14 and AVT-16.

AVT-10: $^1H$ NMR ($\delta$, ppm, $CDCl_3$, Figure S1 in Supporting Information): 0.42−0.69 (m, 2H, j), 0.70−0.95 (m, 4H, i, j′), 1.00−1.20 (m, 4H, h, i′), 1.30−1.43 (m, 2H, h′), 1.45−1.62 (m, 2H, g), 1.63−1.80 (m, 2H, g′), 3.98−4.15 (t, 2H, f), 4.48−4.60 (t, 2H, f′), 5.43−5.58 (d, 1H, $a_1$), 5.80−5.95 (d, 1H, $a_2$), 6.90−7.08 (dd, 1H, b), 7.54−7.60 (d, 1H, e), 7.96−8.03 (d, 1H, d), 8.27−8.36 (s, 1H, c). Anal. Calcd for $C_{20}H_{26}O_4$ (%): C 72.70, H 7.93. Found (%): C 72.31, H 7.91. ZAB-HS mass analysis: 330.

AVT-11: $^1H$ NMR ($\delta$, ppm, $CDCl_3$, Figure S2 in Supporting Information): 0.62−0.75 (m, 2H, k), 0.84−1.00 (m, 4H, j, j′), 1.00−1.18 (m, 4H, i, i′), 1.22−1.39 (m, 4H, h, h′), 1.61−1.76 (m, 4H, g, g′), 4.36−4.40 (t, 2H, f), 4.42−4.50 (t, 2H, f′),5.43−5.50 (d, 1H, $a_1$), 5.80−5.90 (d, 1H, $a_2$), 7.36−7.43 (dd, 1H, b), 7.89−7.93 (d, 1H, e), 7.96−8.00 (d, 1H, d), 8.25−8.30 (s, 1H, c). Anal. Calcd for $C_{21}H_{28}O_4$ (%): C 73.23, H 8.19. Found (%): C 73.34, H 8.41. ZAB-HS mass analysis: 344.

AVT-12: $^1H$ NMR ($\delta$, ppm, $CDCl_3$, Figure S3 in Supporting Information): 0.82−1.02 (m, 4H, k, k′), 1.02−1.20 (m, 4H, j, j′), 1.20−1.40 (m, 4H, i, i′), 1.40−1.59 (m, 4H, h, h′), 1.73−1.92 (m, 4H, g, g′), 4.38−4.60 (m, 4H, f, f′), 5.43−5.58 (d, 1H, $a_1$), 5.80−5.95 (d, 1H, $a_2$), 7.40−7.55 (dd, 1H, b), 7.90−7.99 (d, 1H, e), 7.99−8.09 (d, 1H, d), 8.25−8.38 (s, 1H, c). Anal. Calcd for $C_{22}H_{30}O_4$ (%): C 73.71, H 8.44. Found (%): C 73.94, H 8.47. ZAB-HS mass analysis: 358.

AVT-13: $^1H$ NMR ($\delta$, ppm, $CDCl_3$, Figure S4 in Supporting Information): 1.10−1.21 (s, 6H, k, k′, l), 1.22−1.34 (m, 4H, j, j′), 1.35−1.43 (m, 4H, i, i′), 1.44−1.62 (m, 4H, h, h′), 1.72−1.84 (m, 4H, g, g′), 4.35−4.44 (m, 4H, f, f′), 5.43−5.50 (d, 1H, $a_1$), 5.78−5.85 (d, 1H, $a_2$), 7.44−7.60 (dd, 1H, b), 7.95−8.00 (s, 2H, d, e), 8.29−8.33 (s, 1H, c). Anal. Calcd for $C_{23}H_{32}O_4$ (%): C 74.16, H 8.66. Found (%): C 73.66, H 8.55. ZAB-HS mass analysis: 372.

AVT-14: $^1H$ NMR ($\delta$, ppm, $CDCl_3$, Figure S5 in Supporting Information): 1.20−1.28 (m, 8H, k, k′, l, l′), 1.29−1.40 (m, 4H, j, j′), 1.40−1.50 (m, 4H, i, i′), 1.50−1.59 (m, 4H, h, h′), 1.73−1.86 (m, 4H, g, g′), 4.36−4.45 (m, 4H, f, f′), 5.43−5.50 (d, 1H, $a_1$), 5.76−5.85 (d, 1H, $a_2$), 7.48−7.58 (dd, 1H, b), 7.90−7.99 (s, 2H, d, e), 8.30−8.36 (s, 1H, c). Anal. Calcd for $C_{24}H_{34}O_4$ (%): C 74.58, H 8.87. Found (%): C 74.14, H 8.59. ZAB-HS mass analysis: 386.

**Scheme 1. Synthesis and Polymerization of Alkylidene Vinylterephthalate**

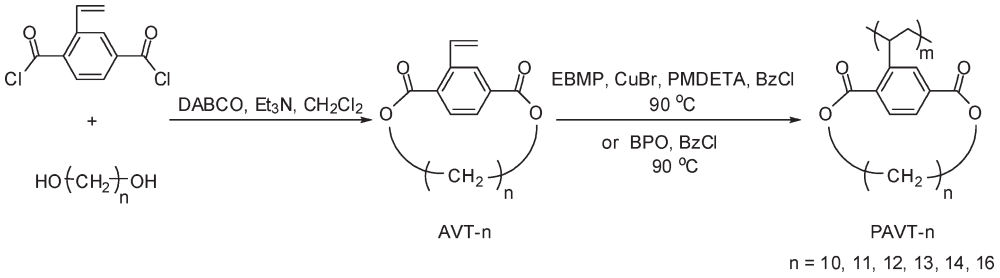


AVT-16: $^1$H NMR ($\delta$, ppm, $CDCl_3$, Figure S6 in Supporting Information): 1.22−1.34 (m, 12H, k, k′, l, l′, m, m′), 1.34−1.44 (m, 8H, i, i′, j, j′), 1.44−1.59 (m, 4H, h, h′), 1.70−1.84 (m, 4H, g, g′), 4.38−4.46 (m, 4H, f, f′), 5.40−5.50 (d, 1H, $a_1$), 5.76−5.89 (d, 1H, $a_2$), 7.40−7.57 (dd, 1H, b), 7.90−7.99 (s, 2H, d, e), 8.25−8.36 (s, 1H, c). Anal. Calcd for $C_{26}H_{38}O_4$ (%): C 75.32, H 9.24. Found (%): C 74.94, H 8.78. ZAB-HS mass analysis: 414.

**Conventional Radical Polymerization.** The conventional radical polymerizations of alkylidene vinylterephthalates (AVT-*n*'s, where *n* is the number of carbon atoms in the side group) were carried out in solution. A typical reaction procedure was as follows. AVT-12 (0.4 g, 1.1 mmol), BPO (0.0014 g, 0.0006 mmol), and chlorobenzene (1.5 g) were successively introduced into a polymerization tube. After three freeze−pump−thaw cycles, the tube was sealed under vacuum and inserted into an oil bath thermostated at 90 °C. The reaction was allowed to continue for 12 h. After the tube was broken to terminate the polymerization, the reaction mixture was diluted with 20 mL of THF and precipitated by dropping the mixture in 200 mL of methanol slowly. The precipitate was collected by filtration and washed with methanol three times and dried at 40 °C under vacuum for 24 h before further characterization. The monomer conversion rate was 98 wt %. The number-average molecular weight and polydispersity of the resultant polymer detected by GPC were $18.8 \times 10^4$ g/mol and 1.58, respectively. $^1$H NMR ($\delta$, ppm, $CDCl_3$): 0.8−1.8 (broad peaks, $-CH_2-$ protons in the backbone and $-CH_2-$ protons in the side chains), 3.1−3.4 (broad peaks, −CH protons in the backbone), 3.7−4.5 (broad peaks, $-OCH_2-$ protons in the side chains), 7.1−7.8 (broad peaks, protons of the phenyl ring).

**Atom Transfer Radical Polymerization (ATRP).** The atom transfer radical polymerization of AVT-12 was carried out in solution. In a typical reaction procedure, AVT-12 (1.0 g, 2.8 mmol), CuBr (0.0020 g, 0.014 mmol), PMDETA (0.0024 g, 0.014 mmol), EBMP (0.0027 g, 0.014 mmol), and chlorobenzene (2.0 g) were successively introduced into a polymerization tube. After three freeze−pump−thaw cycles, the tube was sealed under vacuum and inserted into an oil bath thermostated at 90 °C. The reaction was allowed to continue for 16 h. After the tube was broken to terminate the polymerization, the reaction mixture was diluted with 20 mL of THF and allowed to pass through an $Al_2O_3$ column to separate the catalyst. The polymer was precipitated by dropping the mixture in 200 mL of methanol slowly. The precipitate was collected by filtration, washed with methanol three times and dried at 40 °C under vacuum for 24 h before further characterization. The monomer conversion rate was 90 wt %. The number-average molecular weight and polydispersity of the resultant polymer detected by GPC were $1.7 \times 10^4$ g/mol and 1.18, respectively. $^1$H NMR ($\delta$, ppm, $CDCl_3$): 0.8−1.8 (broad peaks, $-CH_2-$ protons in the backbone and $-CH_2-$ protons in the side chains), 3.1−3.4 (broad peaks, −CH protons in the backbone), 3.7−4.5 (broad peaks, $-OCH_2-$ protons in the side chains), 7.1−7.8 (broad peaks, protons of the phenyl ring).

## Results and Discussion

**Synthesis.** The cyclic monomers, AVT-*n* (*n* = 10−14, 16), were synthesized via the cyclization of vinylterephthaloyl chloride and the corresponding diols in highly dilute solutions (Scheme 1). High-MW linear molecules that precipitated during the reaction process were easily separated by filtration. Because of the large polarity difference with cyclic oligoesters, linear oligomers were readily separated out with a short silica gel column using methylene chloride as the eluent. Only 1 + 1 cyclic compounds were obtained, and no product with larger rings was found in the reaction mixture, which was probably because the two reactive terminals of larger intermediates were difficult to encounter.[19] Reaction conditions, such as temperature, solvent, and concentration, were varied to obtain 1,8-octylidene vinylterephthalate and 1,9-nonylidene vinylterephthalate. Unfortunately, all the efforts failed.

**Table 1. Yields and Energies of AVT-*n* Simulated by Material Studio 5.0 (Accelrys)**

| monomer | energy (kcal/mol) | yield (%) |
|---|---|---|
| AVT-8 | 38.92 | 0 |
| AVT-9 | 35.66 | 0 |
| AVT-10 | 31.04 | 8.4 |
| AVT-11 | 29.40 | 23 |
| AVT-12 | 26.99 | 30 |
| AVT-13 | 21.45 | 35 |
| AVT-14 | 16.80 | 26 |
| AVT-16 | 19.19 | 22 |

It is evident from Table 1 that, under the identical reaction condition, the yield of cyclic monomer increases first with increasing number of methylene groups, reaches a maximum of 35% when *n* = 13, and then decreases when *n* is further increased. Such a size dependence of the reaction yield can be understood from the thermodynamic viewpoint. Table 1 also summarizes the energy of each monomer calculated with Discover Molecular Simulation Program of Material Studio 5.0. The structures of all the molecules were optimized. The energies of the monomers with *n* = 8−10 are clearly larger than others, suggesting that these three compounds with smaller rings are thermodynamically less stable and, as a result, more difficult to obtain. The successful syntheses of the other five monomers with higher yields can thus be rationalized. The decreased yields of AVT-14 and AVT-16 may be due to their larger-ring structures, which make their formation kinetically unfavorable.

The cyclic monomers were characterized by $^1$H NMR, elemental analysis, and mass spectroscopy. All the data completely agreed with the expected structures. Figure 1 exhibits $^1$H NMR spectra of AVT-*n*. The assignment of each resonance peak of AVT-10 is depicted in Figure 1, which was made based on its chemical structure and also by the aid of heteronuclear multiple quantum coherence (HMQC) spectroscopy (Figure 2). It is noted that the $^1$H NMR spectrum of AVT-10 is well resolved, and the resonance signals of the methylene protons f and f′, adjacent to the ester group, are in the regions of 3.98−4.15 and 4.48−4.60 ppm, respectively. When the ring is enlarged, the peaks of f protons shift gradually to the low field, while those

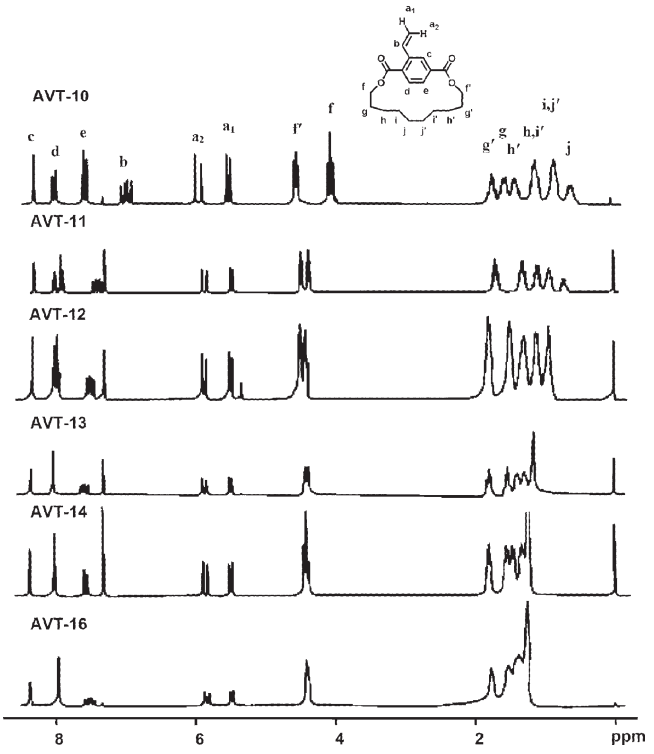


**Figure 1.** $^1$H NMR spectra of alkylidene vinylterephthalate in $CDCl_3$ recorded at room temperature.

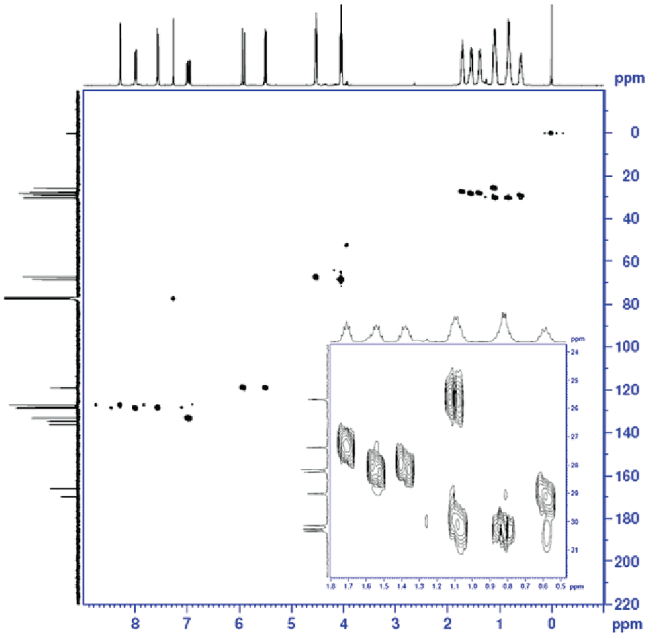


**Figure 2.** Heteronuclear multiple quantum coherence (HMQC) spectrum of AVT-10. The inset refers to the enlargement of the high field.

of f′ protons remain almost in the same region, finally resulting in the merging of resonances corresponding to f and f′ protons for AVT-13 and larger molecules. The vinylic proton b of AVT-10 gives characteristic signals in the region of 6.90−7.08 ppm, which also shift to low field with increasing size of the pendant and reach a stable value with $n$ = 13−16. The aromatic proton e also displays a similar ring-size-dependent chemical shift. In order to understand this interesting phenomenon, nuclear Overhauser effect spectroscopy (NOESY) was performed to

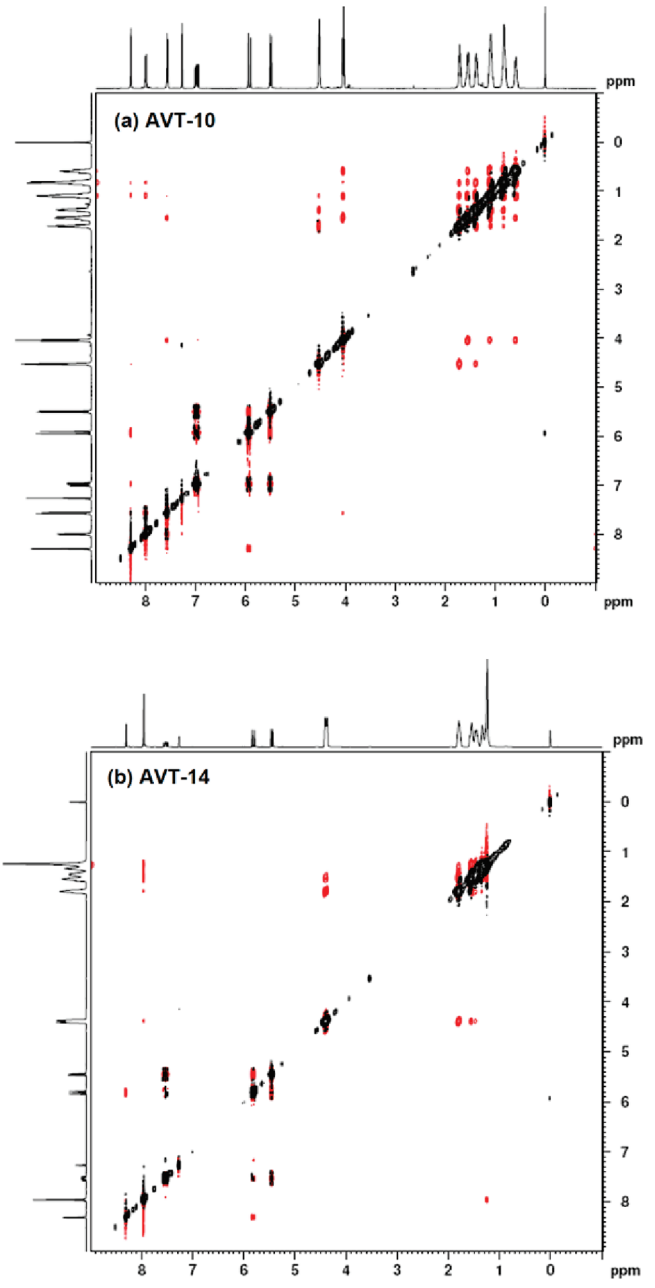


**Figure 3.** Nuclear Overhauser effect spectra (NOESY) of AVT-10 (a) and AVT-14 (b).

investigate the correlation of various protons of AVT-10 and AVT-14 (Figure 3). For AVT-10, the protons f interact with the adjacent protons h, i, and j, while the protons f′ interact only with the protons h′ and i′. In the case of AVT-14, no such difference can be observed. It suggests that the methylene protons linking to ester groups of AVT-10 are in different chemical environments, while those of AVT-14 are in almost identical environments. This might account for the different locations of resonance peaks of the f protons. It has been mentioned in cycloalkanes series[20] that proton resonance peaks of cyclopropane and cyclobutane are significantly different from cycloalkanes with larger sizes. The main difference of this series with more-membered rings from the 3- or 4-membered ring is that the bond angle is greatly different. However, no correlation of vinylic protons with others is discernible for both AVT-10 and AVT-14, implying that other factors may affect the chemical shifts of protons f, b, and e.

Figure 4 illustrates the optimized molecular structures of AVT-10 and AVT-14 by Materials Studio 5.0 (Accelrys). The energies of these two molecules were minimized using geometry optimization, and the Hamiltonian was set as PM6 incorporated in the VAMP Molecular Simulation Program. The torsional angle between the f ester and benzene was about 43° in AVT-10, much larger compared with that of about 26° in AVT-14. Both torsional angles between the f′ ester and benzene in AVT-10 and AVT-14 were a little smaller. It is speculated that the large torsional angle causes poor coplanarity of the ester and benzene, which increases electron density of f protons, makes resonance peaks of f protons shift to the high field, and also lowers the electron density of the vinyl group so that the resonance peaks of b protons shift visibly toward the low field. This was confirmed by the difference between AVT-10 and AVT-14 in NOESY. The larger torsional angle makes protons closer to each other; therefore, f protons were related with protons of the three aliphatic carbons in AVT-10.

**Polymerization.** It is well-known that MW has a significant influence on liquid crystalline property of a polymer.[21] Usually, there is a critical MW for an LC polymer, especially for a main-chain LCP, to generate a mesophase. To investigate the effect of MW on the liquid crystalline properties of the polymers in this work, first we employed ATRP to synthesize poly(1,12-dodecylidene vinylterephthalate) (PAVT-12) with various MWs and relatively narrow polydispersities. The reaction was carried out in BzCl at 90 °C using the CuBr/PMDETA complex as the catalyst and EBMP as the initiator. Table 2 depicts the polymerization results and the properties of the polymers obtained. The absolute number-average molecular weights ranged from $0.75 \times 10^4$ to $12.68 \times 10^4$ g/mol with PDI values lower than 1.3. The GPC traces of the polymers with different molecular weights were monomodal, and the peaks were quite narrow. It is evident that PAVT-12 is able to form a mesophase when its $M_{n,GPC\text{-}LS}$ exceeds $1.07 \times 10^4$ g/mol (corresponding to a degree of polymerization of 30). This will be discussed in detail in the following section.

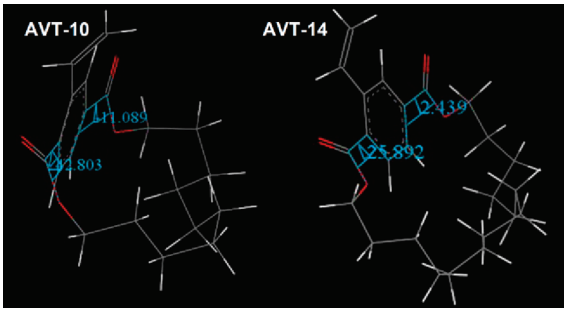


**Figure 4.** Molecular structures of AVT-10 and AVT-14 simulated by Materials Studio 5.0 (Accelrys).

Table 3 lists the conventional polymerization results and the properties of all the resultant polymers. All the cyclic monomers favored radical polymerization, and PAVT-*n*'s with high MWs were obtained in high yields. As the MWs of all the polymers were more than $3.51 \times 10^4$ g/mol, any influence of MW on their liquid crystalline properties could be excluded.

**Thermal Behavior.** All the resultant polymers have quite high thermal stabilities. The temperatures of 5% weight loss are over 370 °C (Tables 2 and 3). Their thermal transition temperatures were evaluated by DSC. A fast heating at a rate of 20 °C/min was employed to measure the annealed polymers, which was performed after the slow cooling (2 °C/min) from 220 °C to room temperature in order to make the glass transition more evident by inducing the endothermic hysteresis peak in the glass transition region. Figure 5 presents the DSC thermograms of PAVT-12 samples with different MWs prepared via ATRP and PAVT-*n*'s obtained via conventional radical polymerization. Only glass transitions can be discerned in the temperature range 30−280 °C. The $T_g$'s of all the polymers are summarized in Tables 2 and 3, separately. In the case of PAVT-12 samples with various MWs, $T_g$ increases first with increasing MW and then reaches a plateau of 156 °C when the $M_{n,GPC\text{-}LS}$ exceeds $5.93 \times 10^4$ g/mol. This is consistent with the general behavior of polymers. It is worth pointing out that $T_g$ of the polymer with a narrow polydispersity is higher than that of the polymer with a broad MW distribution. For example, $T_g$ of PAVT-12-8 obtained via ATRP is 156 °C (Table 2), while that of PAVT-12 obtained from conventional radical polymerization is only 143 °C (Table 3), even though the MW of the latter is much higher than that of PAVT-12-8. This is due to the fact that the polymer with a higher polydispersity value possesses more low-MW components, which significantly lowers the glass transition temperature.

From Table 3, it is evident that the $T_g$ of PAVT-*n* decreases with inceasing size of the side groups in an odd−even manner. The depression of $T_g$ may be rationalized by the enhanced plasticization of cyclic pendants with ring expansion. The alternation behavior is probably related to the variation in side-group architecture caused by odd or even number of methylene groups.

It is worth noting that the $T_g$ of PAVT-*n* is over 100 °C higher than that of PDAVT-*n* (with linear side chains) having the same number of carbon atoms in the side chains.[10] For example,

**Table 2. Polymerization Results and Properties of PAVT-12 Samples with Various Molecular Weights Obtained via Atom Transfer Radical Polymerization**

| polymer[a] | $M_{n,GPC}$[b] ($\times 10^4$ g/mol) | $PDI_{GPC}$[b] | $M_{n,GPC\text{-}LS}$[c] ($\times 10^4$ g/mol) | $PDI_{GPC\text{-}LS}$[c] | $T_g$[d] (°C) | $T_d$[e] (°C) | LC |
|---|---|---|---|---|---|---|---|
| PAVT-12-0 | 0. 38 | 1.09 | 0.75 | 1.03 | 107 | 370 | − |
| PAVT-12-1 | 0.52 | 1.10 | 1.07 | 1.02 | 117 | 378 | + |
| PAVT-12-2 | 0.63 | 1.09 | 1.26 | 1.05 | 122 | 374 | + |
| PAVT-12-3 | 0.95 | 1.12 | 1.97 | 1.03 | 133 | 370 | + |
| PAVT-12-4 | 1.04 | 1.12 | 2.08 | 1.03 | 133 | 371 | + |
| PAVT-12-5 | 1.70 | 1.18 | 3.35 | 1.05 | 139 | 375 | + |
| PAVT-12-6 | 2.86 | 1.24 | 5.66 | 1.08 | 152 | 378 | + |
| PAVT-12-7 | 3.26 | 1.17 | 5.93 | 1.04 | 156 | 376 | + |
| PAVT-12-8 | 5.28 | 1.37 | 12.68 | 1.25 | 156 | 378 | + |

[a] Polymerization condition: chlorobenzene solution (30 wt %); temperature, 90 ± 0.5 °C; [EBMP]:[CuBr]:[PMDETA] = 1:1:1. [b] Number-average molecular weight ($M_{n,GPC}$), weight-average molecular werght ($M_{w,GPC}$), and polydispersity index ($PDI_{GPC} = M_{w,GPC}/M_{n,GPC}$) were obtained by gel permeation chromatography calibrated against polystyrene standards. [c] Number-average molecular weight ($M_{n,GPC\text{-}LS}$), weight-average molecular weight ($M_{w,GPC\text{-}LS}$), and polydispersity index ($PDI_{GPC\text{-}LS} = M_{w,GPC\text{-}LS}/M_{n,GPC\text{-}LS}$) were estimated at 35 °C with a GPC-LS online technique. [d] Glass transition temperature was estimated by differential scanning calorimetry during the second heating process under an inert atmosphere. [e] Temperature at which the weight loss of the polymer reached 5% under an inert atmosphere.

**Table 3. Polymerization Results and Properties of PAVT-*n* Obtained via Conventional Radical Polymerization**

| polymer[a] | $M_{n,GPC}$[b] ($\times 10^4$ g/mol) | $PDI_{GPC}$[b] | $q$ (nm) | $T_g$[c] (°C) | $T_d$[d] (°C) | LC | $d$ (nm) |
|---|---|---|---|---|---|---|---|
| PAVT-10 | 4.30 | 1.70 | 8 | 152 | 370 | + | 1.47 |
| PAVT-11 | 3.51 | 1.77 | 12 | 187 | 368 | + | 1.54 |
| PAVT-12 | 18.8 | 1.58 | 40 | 143 | 371 | + | 1.58 |
| PAVT-13 | 4.89 | 1.93 | 13 | 145 | 373 | + | 1.64 |
| PAVT-14 | 11.1 | 2.78 | 17 | 137 | 371 | − | |
| PAVT-16 | 7.56 | 2.04 | 12 | 118 | 374 | − | |

[a] Polymerization condition: chlorobenzene solution (15 wt %); temperature, 90 ± 0.5 °C; [AVT-*n*]:[BPO] = 200:1. [b] Obtained by gel permeation chromatography calibrated against a series of polystyrene standards. [c] Estimated by differential scanning calorimetry during the second heating process under an inert atmosphere. [d] Temperature at which the weight loss of the polymer reached 5% under an inert atmosphere.

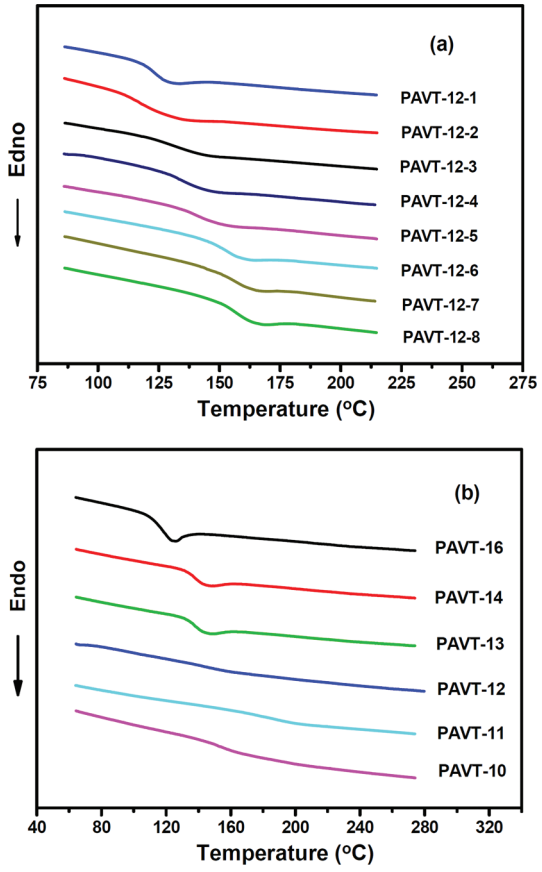


**Figure 5.** Differential scanning calorimetric thermograms of PAVT-12 samples with various molecular weights (a) and PAVT-*n*'s (b).

the $T_g$ of poly[di(*n*-hexyl) vinylterephthalate] (PDAVT-6) is −29.7 °C, while that of PAVT-12 is 143 °C. Generally, the segmental motion of polymer chains begins at $T_g$, which is affected by free volume, chain rigidity, and secondary interactions. The increased $T_g$ of PAVT-*n* with respect to that of PDAVT-*n* can be apprehended from two facts. One is the difference in free volume between these two kinds of polymers. Each repeating unit of PDAVT-*n* has two alkyl ends, while that of PAVT-*n* has no such terminals due to the cyclic structure. The additional end groups of PDAVT-*n* produce extra free volume and, therefore, depress $T_g$ significantly. The other is the greatly increased backbone rigidity caused by the strong steric interaction. This speculation was supported by the large persistence length ($q$) of PAVT-12. For the determination of the persistence length of PAVT-12, six components (PAVT-12a−PAVT-12f) with various MWs and relatively narrow MW distributions were obtained from a PAVT-12 sample with an $M_{n,GPC}$ of $18.8 \times 10^4$ g/mol and a $PDI_{GPC}$ of 1.58 (Table 4). The radius of gyration ($R_g$) and $M_w$ in THF were measured with a

**Table 4. Weight-Average Molecular Weights and Dilute Solution Properties of PAVT-12 Samples with Relatively Narrow MW Distributions**

| run | $M_{w,GPC\text{-}LS}$[a] ($\times 10^4$ g/mol) | $\eta$[a] (mL/g) | $R_g$[a] (nm) |
|---|---|---|---|
| PAVT-12a | 91.2 | 110.1 | 41.8 |
| PAVT-12b | 132.1 | 142.9 | 47.7 |
| PAVT-12c | 203.1 | 185.5 | 57.6 |
| PAVT-12d | 330.3 | 238.6 | 73.6 |
| PAVT-12e | 497.3 | 285.2 | 93.4 |
| PAVT-12f | 645.7 | 316.7 | 111.8 |

[a] Weight-average molecular weights, viscosities, and the radii of gyration were obtained from GPC-LS online technique.

GPC-LS online technique.[22] The persistence length of PAVT-12 is 40 nm evaluated from eq 1

$$R_g^2 = \frac{qL}{3} - q^2 + \frac{2q^2}{L}\left[1 - \frac{q}{L}(1 - e^{-q/L})\right] \quad (1)$$

where $L$ and $q$ are the contour length and the persistence length of the chain, respectively, according to Benoit−Doty theory,[23−25] which indicates an extended main-chain conformation. The extension of the polymer chain caused by the steric requirements of the side chains has also been observed in conventional side-chain LCPs with side-on fixed mesogens[26] as well as in other MJLCPs with linear side chains.[27]

**PLM.** All the polymers are white powders at room temperature. Under the optical microscope with crossed polarizers, they only exhibit faint birefringence presumably due to the poorly ordered structure formed during the precipitation process. When the samples are heated to their $T_g$'s, the weak birefringence disappears immediately. Above $T_g$'s, the polymers behave distinctly different depending on their MWs and the sizes of side groups. As shown in Table 2, no discernible birefringence is developed again by PAVT-12-0 until it thermally decomposes, indicating the absence of ordered structure formation in melt. In the case of the polymers PAVT-12-1−PAVT-12-8, strong birefringence appears immediately above the glass transition and does not vanish on the subsequent heating and cooling processes, indicating the generation of a stable mesophase. Figure 6 shows the texture of PAVT-12-5 under PLM taken at 240 °C, which is the representative image of all the LC polymers of the present work. The influence of the side-group size on the liquid crystalline property can be found in Table 3. The MWs of all the polymers are much larger than the critical MW for PAVT-12 to generate a mesophase, and as a result, the possibility of the low-MW depressing liquid crystallinity can be excluded. Similar to PAVT-12, the other three polymers containing relatively small pendants, i.e., PAVT-10, PAVT-11, and PAVT-13, enter into anisotropic states, which remain on the subsequent heating and cooling processes. When the methylene number of the side group is increased to 14 and 16 as in PAVT-14 and PAVT-16, no fluid with an ordered structure is developed during heating.

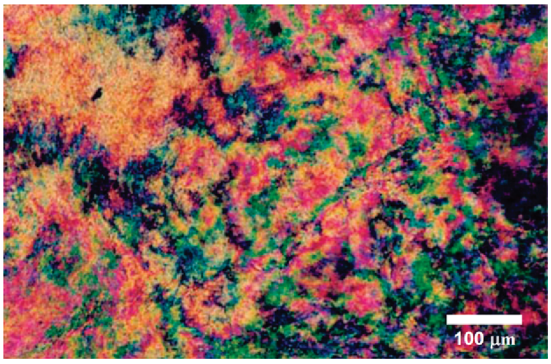


**Figure 6.** Polarized light optical micrograph of PAVT-12-5 in Table 2 taken at 240 °C.

**1D WAXD.** To identify the ordered structures developed in PAVT-*n*'s, 1D WAXD experiments were first performed on the as-cast PAVT-12 samples with various MWs. The powder pattern of PAVT-12-0 exhibited only a scattering halo in the low-angle region, which did not change significantly no matter what thermal process was applied. Figure 7 illustrates the variable-temperature 1D WAXD patterns of PAVT-12-1 (between 3° and 30°) recorded during the first heating and the subsequent cooling steps. At room temperature, only a scattering halo is observed in the low-angle region. When the temperature is above $T_g$, the intensity of the low-angle scattering halo increases. With the temperature further increasing, an intensive diffraction peak appears at $2\theta$ = 5.67° (with a *d*-spacing of 1.56 nm) at 150 °C. At 160 °C, more diffraction peaks appear at higher angles, and the scattering vector ratio of the diffractions follows $1:3^{1/2}:4^{1/2}:7^{1/2}$, demonstrating a long-range-ordered hexagonal lattice.[10] Above 240 °C, the intensity of the diffraction peak decreases but does not disappear even at temperatures over 320 °C, which is in accord with the PLM observation. Upon cooling from 280 °C to room temperature, the sharp low-angle diffraction peak remains almost unchanged along with the higher-order diffractions, implying the mesophase formed is remaining. Figure 7c enlarges the profile of PAVT-12-1 at 220 °C, which displays higher-order diffractions with a scattering vector ratio of $1:3^{1/2}:4^{1/2}:7^{1/2}:9^{1/2}$ for the hexagonal columnar, $\Phi_H$, phase.

PAVT-10, PAVT-11, and PAVT-13 exhibit similar WAXD patterns to those of PAVT-12 and generate $\Phi_H$ phases in melt. It is difficult to confirm whether the side-chain mesogens or the rigid-rod main chains generate LC phases in the case of conventional side-chain LCPs with side-on fixed mesogens. However, in this work, the rigid-rod-like PAVT-*n* polymer chain as a whole serves as a mesogen to form the $\Phi_H$ phases. Polyethylene is also known to form a hexagonal columnar phase at high pressures and high temperatures.[28] Such a mesophase is not found in low-molar-mass LC systems, but also observed in main-chain LCPs.[29] In a sharp contrast, WAXD patterns of PAVT-14 and PAVT-16 only show diffuse halos centered around $2\theta$ = 20°. The *d*-spacing corresponding to the low-angle peak of PAVT-*n* ($n$ = 10−13) increases from 1.47 to 1.64 nm with increasing size of the side group. The *d*-spacing values of poly[di(*n*-pentyl) vinylterephthalates] (PDAVT-5) and poly[di(*n*-hexyl) vinylterephthalates] (PDAVT-6) with linear side chains are 1.52 and 1.63 nm,[12] respectively, much larger than those of PAVT-10 and PAVT-12 which have the same number of carbon atoms in the side groups as PDAVT-5 and PDAVT-6, respectively. It indicates that the polymer main chains of PAVT-*n* with no alkyl ends in the side groups are

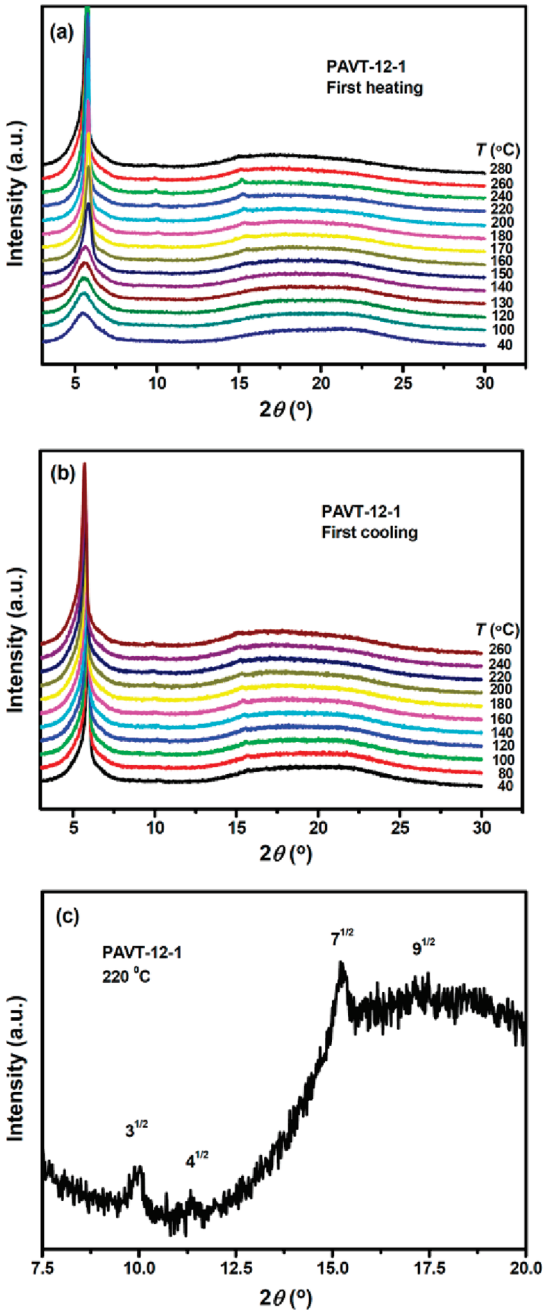


**Figure 7.** One-dimensional wide-angle X-ray diffraction powder patterns of PAVT-12-1 in Table 2 recorded during the first heating (a) and the subsequent cooling (b) courses. Higher-order diffraction peaks (c) recorded at 220 °C are also depicted.

packed tighter than those of PDAVT-*n*. Such a tight packing may also contribute to the much higher $T_g$ of PAVT-*n* compared to that of PDAVT-*n* due to reduced molecular mobility.

It is interesting to compare the critical degrees of polymerization for PAVT-12 with cyclic side chains and PDAVT-6 with linear side chains to form mesophases. These two polymers have the same number of aliphatic carbons in the side chains. From experimental results, for PDAVT-6, more than 200 repeating units are needed to generate a stable mesophase, while 30 repeating units are enough for PAVT-12 to form a $\Phi_H$ phase. This difference can be rationalized by the 1D WAXD results. Every two repeating units along the main-chain axis is estimated to be ~0.50 nm.[11,21] According to Flory's prediction on the basis of his lattice model,[30] for a PAVT-12 cylinder with

a diameter of 1.80 nm, the length of the cylinder should be at least 9.8 nm for the $\Phi_H$ phase to become stable. PAVT-12-1 has 30 repeating units, which corresponds to a length of 7.5 nm (length = 0.5 × 30/2 nm). The diameter of the ring in one repeating unit is 1.2 nm simulated by Material Studio 5.0 (Accelrys) shown in Figure S8 of Supporting Information. Considering the tail effect of the two ends in one PAVT-12-1 chain, the length of one column is ~9.4 nm, which is closed to the theoretical length of 9.8 nm.

The mesophase formation in PDAVT-*n* with linear side chains is an entropy-driven process as poly(di-*n*-alkylsi1oxane)s,[9] in which the free terminals of alkyl chains play an important role in generating ordering of the polymer chains during the heating process. Because of the lack of free alkyl terminals, the entropy effect by the flexible alkyl ends hardly dominates the mesophase formation of PAVT-*n*. On the basis of a much higher $T_g$ for PAVT-*n* and a much lower critical MW for PAVT-*n* to form a mesophase than that for PDAVT-*n*, it is considered that the ordered packing of the PAVT-*n* chains originates from its stiffened nature caused by the steric interaction due to the introduction of the nonmesogenic cyclic pendants. The formation of the LC phases reduces the orientational entropy, but maximizes the positional one, which means that there is still an entropic contribution in generating the LC phases.

## Conclusions

A series of novel vinyl polymers with cyclic pendants, PAVT-*n*'s, were prepared via radical polymerization. Although no traditional mesogenic unit is present in the repeating unit, the polymers display ring-size- and MW-dependent hexagonal columnar phases. Compared with PDAVT-*n* having linear side chains, which has free terminals and can be considered as the open-ring counterpart of PAVT-*n*, PAVT-*n* displays a $T_g$ that is over 100 °C higher, a quite large persistence length, and a much lower critical MW to form a mesophase. In addition, PDAVT-*n* enters into isotropic liquid first when the temperature passes $T_g$ before the formation of a mesophase at temperatures well above $T_g$, whereas PAVT-*n* forms a mesophase immediately above $T_g$. The strong steric interaction due to the introduction of cyclic pendants causes PAVT-*n* to take an extended chain conformation and is considered as the main driving force for the polymer to generate a mesophase. In a sharp contrast, the mesophase formation of PDAVT-*n* is known to be an entropy-driven process, although there is also an entropic contribution in the current cyclic side-chain system. The present work provides a new method to prepare rigid-rod-like objects and build LCPs without employing traditional mesogens. It also magnifies the influence on the properties of the resultant polymer simply by a minimal modification of its side groups. Moreover, the polymers containing cyclic pendants may achieve a noncovalent network with high degrees of freedom in segmental movement utilizing movable cross-linking sites through a threading process,[31,32] which are attracting a lot of interest as new functional materials due to the unusual chemical, physical, and mechanical properties.[33,34]

**Acknowledgment.** The financial support from the National Natural Science Foundation of China (Grants 20774001 and 20834001) and the National Distinguished Young Scholar Fund (Grant 20325415) is gratefully acknowledged.

**Supporting Information Available:** $^1$H NMR spectra of AVT-*n* (*n* = 10−14, 16); molecular structures of AVT-*n* (*n* = 11−13, 16) simulated by Materials Studio 5.0 (Accelrys); $^1$H NMR and $^{13}$C NMR spectra of PAVT-12; 1D WAXD powder patterns of PAVT-*n* (*n* = 10, 11, 13) during the first heating and the subsequent cooling courses; 1D WAXD powder patterns of PAVT-*n* (*n* = 14, 16) during the first heating. This material is available free of charge via the Internet at http://pubs.acs.org.

## References and Notes

(1) Wang, H. M.; Lee, K. W.; Chung, T. S.; Jaffe, M. *Polym. Compos.* **2000**, *21*, 114–123.
(2) Chen, B. K.; Tsay, S. Y.; Chen, J. Y. *Polymer* **2005**, *46*, 8624–8633.
(3) Kikuchi, H.; Sato, H.; Fujikake, H.; Sato, F. *IEEE Ind. Appl. Soc. Ann. Meeting* **2008**, *1*−*5*, 442–446.
(4) Caputo, R.; De Luca, A.; De Sio, L.; Pezzi, L.; Strangi, G.; Umeton, C.; Veltri, A.; Asquini, R.; d'Alessandro, A.; Donisi, D.; Beccherelli, R.; Sukhov, A. V.; Tabiryan, N. V. *J. Opt. A: Pure Appl. Opt.* **2009**, *11*, 024017.
(5) Cupelli, D.; Nicoletta, F. P.; Manfredi, S.; Vivacqua, M.; Formoso, P.; De Filpo, G.; Chidichimo, G. *Sol. Energy Mater. Sol. Cells* **2009**, *93*, 2008–2012.
(6) Kwon, Y. K.; Chvalun, S.; Schneider, A. I.; Blackwell, J.; Percec, V.; Heck, J. A. *Macromolecules* **1994**, *27*, 6129–6132.
(7) Percec, V.; Ahn, C. H.; Barboiu, B. *J. Am. Chem. Soc.* **1997**, *119*, 12978–12979.
(8) Buchowicz, W.; Holerca, M. N.; Percec, V. *Macromolecules* **2001**, *34*, 3842–3848.
(9) Out, G. J. J.; Turetskii, A. A.; Moller, M.; Oelfin, D. *Macromolecules* **1994**, *27*, 3310–3318.
(10) Yin, X. Y.; Ye, C.; Ma, X.; Chen, E. Q.; Qi, X. Y.; Duan, X. F.; Wan, X. H.; Cheng, S. Z. D.; Zhou, Q. F. *J. Am. Chem. Soc.* **2003**, *125*, 6854–6855.
(11) Tu, H. L.; Wan, X. H.; Liu, Y. X.; Chen, X. F.; Zhang, D.; Zhou, Q. F.; Shen, Z. H.; Ge, J. J.; Jin, S.; Cheng, S. Z. D. *Macromolecules* **2000**, *33*, 6315–6320.
(12) Tang, H.; Cao, H. Q.; Zhu, Z. G.; Wan, X. H.; Chen, X. F.; Zhou, Q. F. *Polymer* **2007**, *48*, 4252–4263.
(13) Guan, Y.; Chen, X. F.; Shen, Z. H.; Wan, X. H.; Zhou, Q. F. *Polymer* **2009**, *50*, 936–944.
(14) Percec, V.; Rodenhouse, R. *Macromolecules* **1989**, *22*, 4408–4412.
(15) Tuffin, P. P.; Toyne, K. J.; Goodby, J. W. *J. Mater. Chem.* **1995**, *5*, 2093–2104.
(16) Tu, H. L.; Zhang, D.; Wan, X. H.; Chen, X. F.; Liu, Y. X.; Zhang, H. L.; Zhou, Q. F. *Macromol. Rapid Commun.* **1999**, *20*, 549–551.
(17) Zhang, D.; Liu, Y. X.; Wan, X. H.; Zhou, Q. F. *Macromolecules* **1999**, *32*, 4494–4496.
(18) Zhang, D.; Liu, Y. X.; Wan, X. H.; Zhou, Q. F. *Macromolecules* **1999**, *32*, 5183–5185.
(19) Hall, A. J.; Hodge, P.; McGrail, C. S.; Rickerby, J. *Polymer* **2000**, *41*, 1239–1249.
(20) Burke, J. J.; Lauterbur, P. C. *J. Am. Chem. Soc.* **1964**, *86*, 1870–1871.
(21) Ye, C.; Zhang, H. L.; Huang, Y.; Chen, E. Q.; Lu, Y. L.; Shen, D. Y.; Wan, X. H.; Shen, Z. H.; Cheng, S. Z. D.; Zhou, Q. F. *Macromolecules* **2004**, *37*, 7188–7196.
(22) Yanagisawa, M.; Isogai, A. *Biomacromolecules* **2005**, *6*, 1258–1265.
(23) Benoit, H.; Doty, P. *J. Phys. Chem.* **1954**, *57*, 958–963.
(24) Kashiwagi, Y.; Norisuye, T.; Fujita, H. *Macromolecules* **1981**, *14*, 1220–1225.
(25) Sato, T.; Norisuye, T.; Fujita, H. *Macromolecules* **1984**, *17*, 2696–2700.
(26) Thomsen, D. L.; Keller, P.; Naciri, J.; Pink, R.; Jeon, H.; Shenoy, D.; Ratna, B. R. *Macromolecules* **2001**, *34*, 5868–5875.
(27) Chen, X.-F.; Shen, Z.; Wan, X.-H.; Fan, X.-H.; Chen, E.-Q.; Ma, Y.; Zhou, Q.-F. *Chem. Soc. Rev.* **2010**, *39*, 3072–3101.
(28) Bassett, D. C.; Turner, B. *Philos. Mag.* **1974**, *29*, 285–307.
(29) Fitzgerald, J. J.; Noonan, J. M.; Kapitza, H.; Zentel, R. *Polymer* **1991**, *32*, 2244–2251.
(30) Flory, P. J. *Proc. R. Soc. London, Ser. A* **1956**, *234*, 73–89.
(31) Gong, C. G.; Gibson, H. W. *J. Am. Chem. Soc.* **1997**, *119*, 5862–5866.
(32) Gong, C. G.; Gibson, H. W. *J. Am. Chem. Soc.* **1997**, *119*, 8585–8591.
(33) Ichi, T.; Watanabe, J.; Ooya, T.; Yui, N. *Biomacromolecules* **2001**, *2*, 204–210.
(34) Fleury, G.; Schlatter, G.; Brochon, C.; Travelet, C.; Lapp, A.; Lindner, P.; Hadziioannou, G. *Macromolecules* **2007**, *40*, 535–543.